97-GT-394

THE AMERICAN SOCIETY OF MECHANICAL ENGINEERS
345 E. 47th St., New York, N.Y. 10017

96-GT-394

BLOCKAGE DEVELOPMENT IN A TRANSONIC, AXIAL COMPRESSOR ROTOR

Kenneth L. Suder
NASA-Lewis Research Center
Cleveland, Ohio

ABSTRACT

A detailed experimental investigation to understand and quantify the development of blockage in the flow field of a transonic, axial flow compressor rotor (NASA Rotor 37) has been undertaken. Detailed laser anemometer measurements were acquired upstream, within, and downstream of a transonic, axial compressor rotor operating at 100%, 85%, 80%, and 60% of design speed which provided inlet relative Mach numbers at the blade tip of 1.48, 1.26, 1.18, and 0.89 respectively. The impact of the shock on the blockage development, pertaining to both the shock / boundary layer interactions and the shock / tip clearance flow interactions, is discussed. The results indicate that for this rotor the blockage in the endwall region is 2–3 times that of the core flow region, and the blockage in the core flow region more than doubles when the shock strength is sufficient to separate the suction surface boundary layer.

NOMENCLATURE

A	Area, m^2
B	Blockage, (1-effective flow area/geometric flow area)
H	Shape factor, $H=\delta^*/\theta$
M_{rel}	Relative Mach number
N	Rotation speed of rotor, rpm
NB	Number of rotor blades, 36
P	Total Pressure, N/m^2
P_{ref}	Standard day total pressure, 101325 N/m^2
r	Radius, cm
T_{ref}	Standard day total temperature, 288.2 K
T_s	Static Temperature, K
u	Local Velocity, m/s
y	Distance normal from a surface, cm
δ	Boundary layer thickness, cm
δ^*	Boundary layer displacement thickness, cm
θ	Boundary layer or wake momentum thickness, cm
ρ	Density, kg/m^3

INTRODUCTION

Based on the work of Koch and Smith (1976, 1981), it is clear that there is a relationship between the blockage (defined as the effective reduction in flow area) in a turbomachine and the losses, pressure rise, and flow range of that turbomachine. For example, Smith (1970) correlated the casing boundary layer displacement thickness to the static pressure rise and efficiency from a number of low speed multistage compressor tests. Furthermore, Smith demonstrated that for low speed axial compressors the endwall boundary layer thickness is directly related to 1) the blade-to-blade passage width, 2) the aerodynamic loading level, and 3) the tip clearance. Smith never used the term blockage, but his work clearly demonstrates the direct relationship of the blockage to the pressure rise and losses in the endwall region of low speed compressors. In this investigation both endwall blockage and the blockage generated by the blade surface boundary layers will be evaluated. It will be shown that the blockage resulting from the blade boundary layers is sensitive to the inlet Mach number level, especially at high Mach number conditions for which the shock may induce boundary layer separation, thereby changing the blockage level and its spanwise distribution.

A methodology to quantify the endwall blockage generated within the blade row by the tip clearance flow was developed by Khalid (1994). His results were based on three-dimensional Navier-Stokes computations of the flowfields in a low speed stator, low speed rotor, and a transonic fan with several values of tip clearance height. His results indicated that the loss in total pressure in the endwall region resulted from the interaction of the leakage flow and passage flows and that the vortical structure associated with the clearance vortex was not a major factor in generating the endwall blockage. Khalid developed a correlation between the endwall blockage and the aerodynamic loading on the blade which indicated there is a limiting value of the loading. In this paper we use experimental data and variations on Khalid's methodology to evaluate the blockage in both the endwall and core flow regions of a high speed, highly loaded compressor rotor. The assumptions made and calculation procedure

Presented at the International Gas Turbine & Aeroengine Congress & Exhibition
Orlando, Florida — June 2–June 5, 1997
This paper has been accepted for publication in the Transactions of the ASME
Discussion of it will be accepted at ASME Headquarters until September 30, 1997

used in this paper to estimate blockage are described in the data analysis section.

One may question the need to quantify blockage from experimental measurements with the advent of three-dimensional Navier-Stokes flow solvers. However, it has been demonstrated that state-of-the-art computational fluid dynamic (CFD) codes are unable to accurately predict the performance and flowfield characteristics of NASA Rotor 37. CFD simulations of Rotor 37 generated for the ASME 'blind test case study' as well as additional simulations of Rotor 37 generally predict a higher total pressure and total temperature rise across the rotor as compared to the experimental data. (See Chima, 1996, Dalbert and Wiss, 1995, Denton, 1996, Shabbir et al., 1996, and Suder, 1996.) In addition, the shapes of the radial distributions of total temperature and pressure from the CFD simulations were very much different from that of the experimental data. These discrepancies between the data and CFD and the differences among the various CFD solutions are in part attributed to the inability of the CFD to accurately predict the blockage and to the sensitivity of the rotor's performance to slight changes in blockage. Further evidence that the CFD has difficulty in accurately predicting the blockage in NASA Rotor 37 can be found in the results of Suder & Celestina (1996) who studied the interaction between the shock and tip clearance flow. Their results indicated that their CFD simulation predicted the features and trends of the endwall flow field but underpredicted the radial penetration of the tip clearance flow. It was surmised that the CFD was underpredicting the blockage in the endwall region. In this paper we will quantify the blockage development resulting from the shock / tip clearance flow interactions and the shock / blade surface boundary layer interactions and relate the blockage to the performance characteristics of the rotor.

To illustrate the impact of the blockage on the performance characteristics of the rotor in this investigation using only the experimental data, the measured and ideal pressure rise and adiabatic efficiency characteristics for this test compressor operating at design speed are plotted in Figure 1. The mass flow is normalized by the choking mass flow of 20.93 kg/s. The ideal pressure ratio was calculated by using the isentropic relation and the actual work input. The shock loss was calculated using a normal shock with an inlet Mach number of 1.4. In a transonic / supersonic compressor the shock is the primary source of pressure rise, and though the losses are considerable across the shock, it is shown in Figure 1 that the shock is an efficient compressor. These results are consistent with the findings of Wood et al. (1986). The remaining losses such as those due to blade boundary layers, blade wakes, secondary flows, and tip clearance flows are indicative of a blockage to the flow, and they will be referred to as the "blockage related losses". It is evident that for this rotor the blockage has a considerable impact on the performance, and there is much potential for gains in machine performance if we can understand the blockage development and optimize the design to minimize the blockage related losses.

Therefore, the intent of this work is to quantify the level of blockage and to explain and verify with experimental evidence the flow mechanisms responsible for the development of blockage in a transonic, axial compressor rotor operating at design and off-design conditions. Previous research in this area has either been performed using computational methods to calculate the flowfield or experimental measurements acquired downstream of the compressor—generally

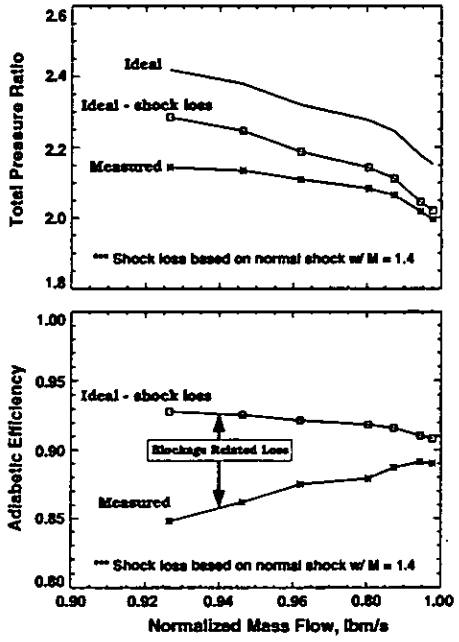

Figure 1 Estimation of blockage related losses and their impact on performance.

for low speed machines operating at design conditions. In this investigation detailed laser anemometer measurements acquired upstream, within, and downstream of a transonic, axial compressor rotor operating at design and off-design conditions are used to investigate blockage development. At design speed where the rotor shock is present, data is presented and analysis performed at two operating conditions to show the blockage development within and downstream of the rotor blade row. Inside the blade row the blockage is evaluated ahead of the rotor passage shock, downstream of the rotor passage shock, and near the trailing edge of the blade row. This analysis is performed in the core flow area as well as in the casing endwall region. Blockage is also evaluated for two part speed conditions for which 1) the rotor passage shock is much weaker than that at design speed and 2) there is no rotor passage shock.

TEST EQUIPMENT & PROCEDURE

Facility and Test Rotor. The experiment was performed in the single stage transonic compressor facility at the NASA Lewis Research Center. A detailed description of the facility is given by Urasek and Janetzke (1972). The test compressor was designed as an inlet stage for an eight-stage 20:1 pressure ratio advanced core compressor and is designated as NASA Stage 37. For this experiment NASA Rotor 37 was tested in isolation to avoid the interaction effects generated by the presence of an upstream inlet guide vane or downstream stator blade row. (Note that this test configuration of NASA Rotor 37 was that used as the test vehicle for the ASME sponsored CFD testcase exercise. The results of this exercise were presented at the 1994 ASME IGTI turbomachinery conference and are discussed by Denton, 1996.) The rotor design pressure ratio is 2.106 at a mass flow of 20.19 kg/s. The inlet Mach number is 1.13 at the hub and 1.48 at the tip at the design tip speed of 454 m/s. The rotor aspect ratio is 1.19 and the hub/tip radius ratio is 0.70. Details

Table 1 Variation of Inlet Relative Mach Number and rotor tip clearance for tested rotor wheel speeds.

% Design Speed	M_{rel} at Hub	M_{rel} at Tip	Tip Clearance, mm (% rotor tip chord)
60	0.68	0.89	0.58 (1.0)
80	0.90	1.18	0.50 (0.9)
85	0.96	1.26	N/A
100	1.13	1.48	0.40 (0.7)

of the rotor aerodynamic design were reported by Reid and Moore (1978). Overall aerodynamic performance of the stage was reported by Moore and Reid (1980).

Aerodynamic Probe Measurements. The performance characteristics of the rotor are determined from aerodynamic probes which are surveyed radially approximately one chord upstream of the rotor and two chords downstream of the rotor. The probe measurements are corrected for Mach number and streamline slope based on a calibration of each probe used and on the design streamline slope. All measurements are corrected to NACA standard-day sea-level conditions at the rotor inlet. Radial distributions of total temperature are mass averaged across the annulus. Radial distributions of total pressure are energy averaged by converting them to their enthalpy equivalents and then mass averaging them across the annulus. The details of these calculations are described by Suder (1996). The measurement uncertainties are: massflow, ±0.3 kg/s; flow angle, ±1.0 degrees; total pressure, ±0.01 N/cm^2; total temperature, ±0.6K.

Laser Anemometer System & Measurements. Detailed flow field measurements are acquired with a two color fringe-type laser anemometer system which is configured to simultaneously acquire the tangential and axial velocity components. Measurements are acquired along the 30%, 50%, 70%, 90%, and 95% span streamsurfaces and several cross-channel planes upstream and downstream of the rotor. A full description of the laser anemometer system, seeding system, data acquisition and reduction procedure is given in Suder (1996). The uncertainties in the laser anemometer velocity and flow angle measurements are estimated as 1% and 0.5 degrees, respectively.

All laser anemometer results presented are based on the velocity distribution across an averaged blade passage, which is calculated by ensemble-averaging the measurements acquired in each individual blade passage. The relative Mach number is calculated from the relative velocity and the local speed of sound at each point in the flow field using the procedure discussed by Strazisar (1989).

Experimental Procedure. The majority of the data were acquired for the rotor operating at design speed conditions. However, to evaluate the effect of the inlet Mach number on the rotor performance and blockage development, data were also acquired at part speed conditions. The inlet relative Mach numbers and measured tip clearance for each rotor wheel speed are provided in Table 1.

The performance characteristics at 60%, 80%, and 100% of design speed, based on the aerodynamic probe surveys, are plotted in Figure 2. Detailed laser anemometer surveys were performed at one throttle valve setting each for the data acquired at 60%, 80%, and 85% of rotor design speed. At design speed the LFA data were acquired at three throttle valve positions and are denoted max flow,

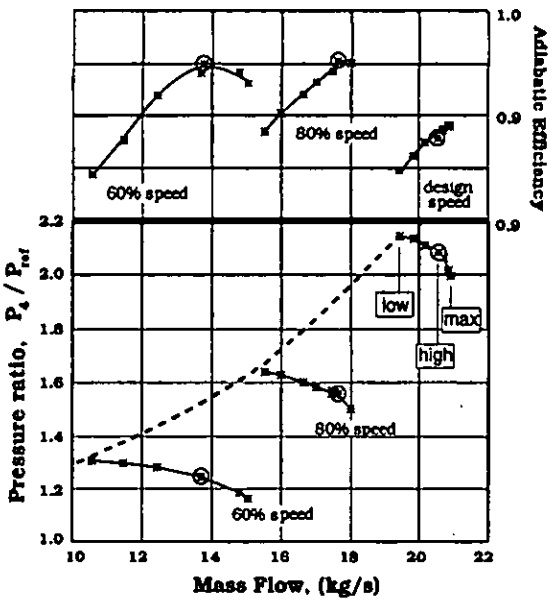

Figure 2 Overall Performance Characteristics.

high flow, and low flow in reference to the amount of mass flow through the rotor. The circled data points in Figure 2 indicate the high flow operating conditions where the detailed laser anemometer surveys were acquired. These conditions represent a nearly constant incidence angle to the rotor at 60%, 80%, and 100% of design speed.

DATA ANALYSIS : QUANTIFICATION OF BLOCKAGE

Blockage is defined as an effective reduction in flow area and is represented by:

$$B = \left[1 - \left(\frac{effective\ area}{geometric\ area}\right)\right] = 1 - \frac{(A - \int \delta^* dr)}{A} \qquad (1)$$

where A is the total area and δ^* is the integral of the velocity-density deficit across the rotor passage. The integral of the velocity-density deficit is defined at each radial measurement location by

$$\delta^*(r) = \int_{\theta=0}^{2\pi/NB} \left(1 - \frac{\rho u}{(\rho u)_{inviscid}}\right) r d\theta \qquad (2)$$

and is analogous to the displacement thickness from boundary layer theory. (δ^* will be referred to as the displacement thickness throughout the text.) The difficulty in evaluating δ^* arises in determining the inviscid velocity and density inside a compressor, in which the flow is compressible and not uniform across the passage. Since the density is not measured by the laser anemometer system, an approximation of the displacement thickness inside the blade row is evaluated by neglecting the variation of density within the defect region , i.e. it is assumed that $\rho = \rho_{inviscid}$, and the displacement thickness is estimated by:

$$\delta^*(r) = \int_{\theta=0}^{2\pi/NB} \left(1 - \frac{u}{u_{inviscid}}\right) r d\theta \qquad (3)$$

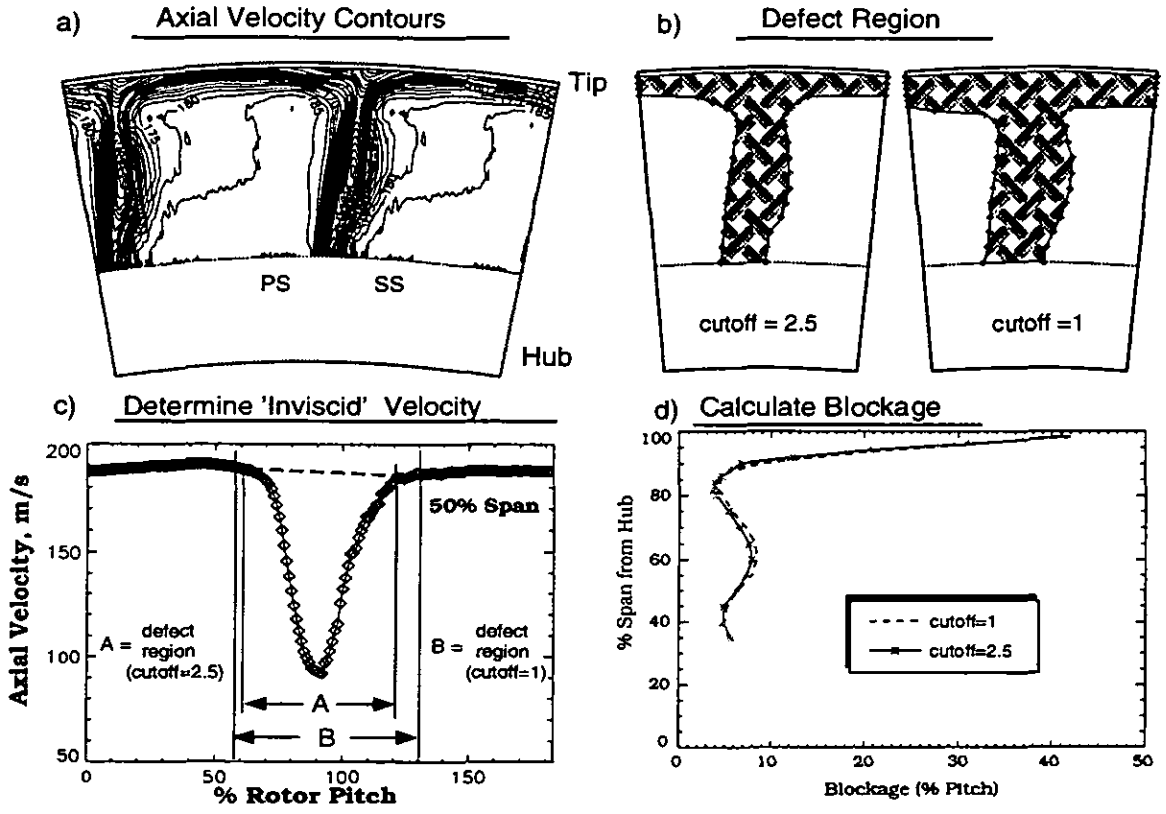

Figure 3 Procedure to calculate blockage downstream of the blade row.

Downstream of the blade it is assumed that the static pressure is constant within the defect region and is equal to the value at the edge of the defect region. Assuming uniform static pressure in the defect region in conjunction with the ideal gas law, the displacement thickness downstream of the blade is estimated by:

$$\delta^*_{downstream}(r) = \int_{\theta=0}^{2\pi/NB} \left(1 - \frac{T_{s,\,inviscid} \cdot u}{T_s \cdot u_{inviscid}}\right) r d\theta \qquad (4)$$

The displacement thickness downstream of the blade has been evaluated using both equation 3 and equation 4. Comparing these calculations to those from CFD results indicate that using equation 4 is appropriate to account for the density variations in the defect region. (The analysis code used in the present study was used by Suder and Celestina (1996), and it solves the Reynolds-Averaged form of the Navier-Stokes equations developed by Adamczyk (1989).) In order to assess the impact of the density variations in the defect region on the blockage calculations, this same CFD simulation was used to calculate the blockage using both the density-velocity defect (equation 2) and the velocity defect alone (equation 3). These calculations (though not shown herein) indicate the region of velocity defect is in phase with density defect, therefore the shape of the curve depicting the radial distribution of blockage is the same whether or not density is included in the calculation of displacement thickness. However, the inclusion of density variations in the blockage calculation does increase the overall level of blockage, and for this case the difference in blockage was only 0.8% of the flow area. Also, note that CFD users can calculate the blockage using the same procedure used herein to compare their results to the data. In summary, the values of blockage calculated downstream of the rotor using only the measured velocity distributions are believed to be within 10% of those calculated with density variations included, which is sufficient to establish trends and evaluate the regions of the flowfield which dominate the generation of blockage.

Quantification of Blockage Downstream of the Rotor Blade Row

Downstream of the rotor blade row, blockage is evaluated at a given axial location by calculating the displacement thickness for each radial location at which data were measured. An example illustrating the method used is presented in Figure 3.

1: ***Identify the area over which to evaluate the blockage.*** Figure 3a is a cross-channel plot of the axial velocity contours at approximately 15% rotor chord downstream of the rotor trailing edge. The data were ensemble and passage averaged and were then duplicated across two rotor pitches in the circumferential direction for clarity. In this example the data were acquired from 35% to 98% of span from the rotor hub. The axial velocity contours are shown for increments of 5 m/s and the velocity deficit due to the rotor wake and endwall flow is clearly identifiable.

2: ***Identify the velocity defect region.*** The defect region is determined by taking the gradient of the axial velocity in the radial

and circumferential directions and applying a cutoff value:

$$Defect\ Region:\ where \left|\frac{\partial u}{\partial r}\right| + \left|\frac{\partial u}{\partial (r\theta)}\right| \geq (cutoff) \quad (5)$$

The cutoff value is influenced by the radial spacing of the measurements and the velocity gradients within the flowfield. In this investigation the radial spacing of the measurements was identical for each survey. However, the velocity gradients within the flowfield varied with operating condition and a different cutoff value was subjectively selected for each case. Although the determination of this cutoff value is arbitrary, its choice does not significantly impact the evaluation of the displacement thickness for two reasons. First, the velocity gradients decrease significantly with distance from the center of the defect region to the outer edges of the defect region. Second, outside of the defect region the velocity gradients are less than those within the defect region as is evident from the velocity contours in Figure 3a. The sensitivity of the defect region size to the cutoff value is shown in Figure 3b, where the defect region has been roughly centered on the plot. A comparison of the axial velocity contours in Figure 3a to the defect region in Figure 3b illustrates that this method of determining the defect region is reasonable.

3: ***Determine the 'inviscid' velocity at each measurement location.*** Outside of the defect region the 'inviscid' velocity is set equal to the local velocity. In the core flow region (the region in which the velocity defect no longer encompasses the entire circumference), the inviscid velocity across the defect region is linearly extrapolated from the velocity distribution in the circumferential direction outside of the defect region. This is shown schematically in Figure 3c, which includes the distribution of axial velocity at 50% span and the location of the defect region. The dashed line indicates the estimated 'inviscid' velocity distribution which would be present if there were no viscous effects. Since the variation in the velocity between the pressure surface and the suction surface side of the wake is small in comparison to the velocity deficit within the wake, the calculation of the displacement thickness is insensitive to the estimation of the inviscid velocity. This process breaks down in the endwall region where the velocity defect encompasses the entire circumference. Therefore, in the endwall defect region the inviscid velocity is extrapolated in the radial direction from the velocity distribution outside of the defect region.

4: ***Calculate the blockage at each radial measurement location.*** The blockage was calculated in a two-dimensional sense in that the displacement thickness is calculated at each radial measurement location and divided by the circumferential distance corresponding to the rotor pitch at that radial location. The results, presented in Figure 3d, indicate that the blockage is not a strong function of the cutoff value. The radial distribution of the blockage is identical in shape for both values of the cutoff and the maximum difference in the blocked area is about 0.8% of blade pitch. For all cases used in this investigation, the cutoff value ranged between 2 sec^{-1} and 3 sec^{-1}. Note that the resulting radial distribution of blockage is consistent with the measured velocity field. For example, the local increase in blockage centered around 60% span coincides with the increased wake width identified in Figure 3a.

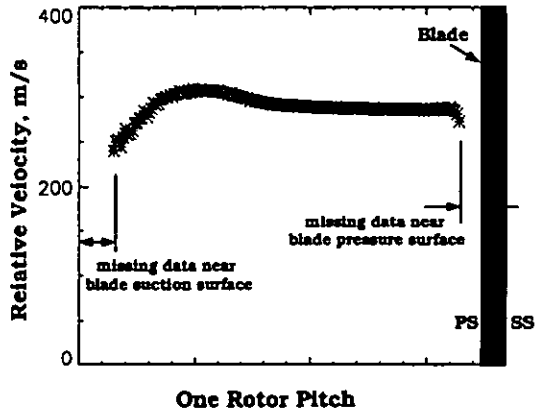

Figure 4 Pitchwise relative velocity distribution at 85% chord, 70% span for the rotor operating at design speed low flow condition.

Quantification of Blockage within the Rotor

Within the rotor the boundary layer is thick enough to enable acquisition of measurements within the outer region of the boundary layer. For example the relative velocity across a rotor pitch at approximately 85% rotor chord and 70% rotor span is plotted in Figure 4. The left hand side of the plot represents the suction surface of a rotor blade and the next blade is shaded on the right hand side of the plot. There is no data within about 8% of pitch from the suction surface and about 5% of pitch from the pressure surface. Clearly, the suction surface boundary layer contributes substantially more to the blockage development as compared to the pressure surface boundary layer. In order to estimate the velocities within the inner region of the boundary layer where the data is missing and hence calculate the blockage, the following steps were taken:

1. Identify the edge of the boundary layer in a manner similar to that described in the previous section for finding the edges of the wake.
2. Fit a power law velocity distribution to the data in the outer region of the boundary layer by determining the value of the exponent 'n' for:

$$\frac{u}{u_{inviscid}} = \left(\frac{y}{\delta}\right)^n \quad (6)$$

3. Use the power law fit to estimate the values of the velocity within the inner region of the boundary layer where no data was acquired.
4. Calculate the displacement and momentum thicknesses using the measured and estimated velocities within the boundary layer. The resulting shape factor is compared to the theoretical value of the shape factor H, where H=2n+1 (Schlichting, 1979)), to assess the 'goodness' of the power law fit described in item 2.
5. Calculate the blockage. To obtain a dimensionless blockage the displacement thickness is normalized by the rotor gap (the distance corresponding to one rotor pitch minus the blade thickness).

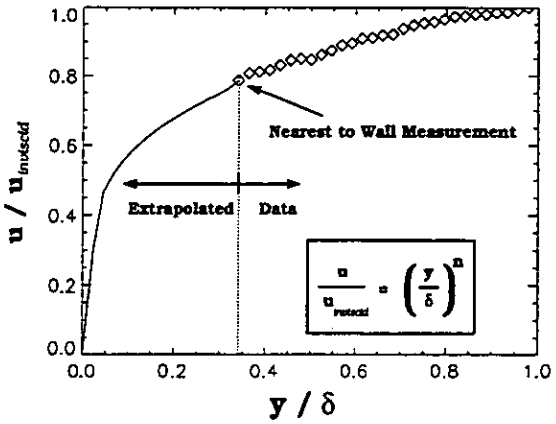

Figure 5 Sample calculation showing estimation of boundary layer parameters.

The result of this calculation procedure for the suction surface boundary layer shown in Figure 4 is presented in Figure 5. The shape factor calculated from the data is 1.55 versus the theoretical value of 1.48 which was based on the power law velocity distribution. The fact that the value for the shape factor is reasonable for a turbulent boundary layer in an adverse pressure gradient and that the shape factor from the idealized power law velocity distribution differs by about 5% from the measured data indicate that approximating the velocity profile with a power law is a reasonable approach. In Figure 6, the calculated boundary layer parameters for the low flow design speed condition at 70% span are plotted in relation to the blade geometry. Note that at each axial measurement location the boundary layer parameters are calculated independently, yet as a group they appear well-behaved. In the following section these procedures will be used to calculate the blockage development within the blade row.

RESULTS AND DISCUSSION OF BLOCKAGE ESTIMATIONS

The objective in this section is to quantify the blockage generated in a transonic compressor rotor operating at design and part speed conditions. The rotor flow field is arbitrarily divided into the core-flow region and the endwall region. Suder & Celestina (1996) reported that the radial extent of influence of the tip clearance flows was limited to the outer 15–20% span for this rotor. Therefore, the endwall region (primarily the tip region for our discussions) is defined as the outer 15–20% span. Similarly, the core-flow region, which is defined as the region outside of the influence of the tip clearance flows and endwall boundary layers, encompasses the 20–80% span region of the compressor flowpath. The blockage in the core flow region will be quantified both downstream and within the rotor blade row where the data is of sufficient detail. In the endwall region, where the flow gradients are large in the radial, circumferential, and axial directions, there is not sufficient data in the radial direction to assess the blockage within the blade row. Therefore, the endwall blockage will be quantified downstream of the rotor only, and the results will be compared to Khalid's correlation (Khalid, 1994) of blockage parameter versus loading parameter.

Downstream Blockage Calculations

At the trailing edge of the blade the boundary layers from the pressure and suction surface merge to form the rotor wake.

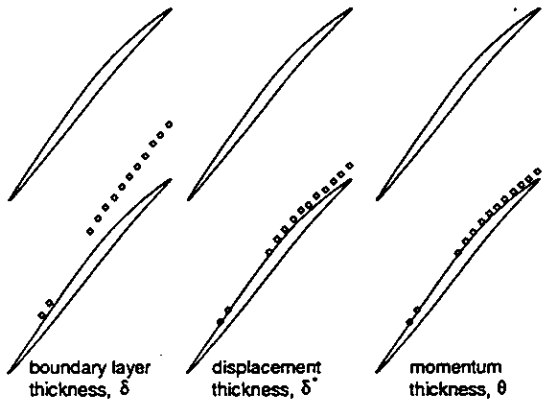

Figure 6 Development of the boundary layer thickness parameters, δ, δ^*, and θ for the low flow, design speed condition at 70% span.

In the near wake region, there is significant momentum exchange and mixing between the two blade surface boundary layers. The streamwise extent of this near wake mixing region was determined by Suder (1996). In the present investigation, the blockage is evaluated downstream of this mixing region. At design speed conditions the blockage will be evaluated at 130% chord. At part speed conditions there is insufficient data at 130% chord and the blockage will be evaluated at 115% chord. For the high flow condition at 100% speed the blockage distribution at 115% chord is nearly identical to that at 130% chord, therefore using either of these two locations is considered appropriate.

Comparison of Results at 100%, 80%, and 60% Rotor Speed. The impact of the inlet relative Mach number on the blockage development is illustrated in Figure 7, where the radial distributions of blockage are plotted for the rotor operating at mass flows which maintain nearly the same flow incidence angle. These operating conditions are near peak efficiency and correspond to the circled conditions in Figure 2. The symbols for the design speed results indicate the measurement radii. These same measurement locations were used at 60% and 80% speed, but the symbols were omitted for clarity. For part speed conditions the following observations are noteworthy:

1. Blockage in the endwall region is much larger than the core region.
2. Blockage in the endwall region is slightly higher for the 80% speed case as compared to the 60% speed case. Although the casing boundary layer is thicker and the tip clearance height is greater at 60% speed, the blockage generated by the tip clearance flow is larger at 80% speed due to 1) the higher blade loading which results in more flow through the tip clearance gap and 2) the interaction of the tip clearance vortex with the passage shock.
3. Blockage in the core region is nearly identical at 60% and 80% speed which implies the blockage due to the blade wake is nearly identical at 60% and 80% speed.
4. The radial distribution of blockage in the core region is nearly constant with span.

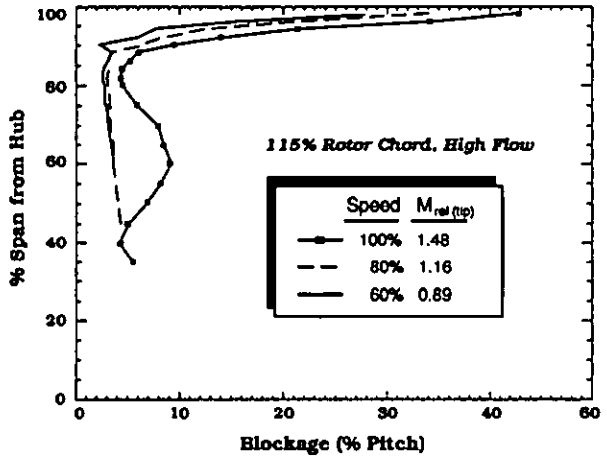

Figure 7 Radial distribution of Blockage at 60%, 80%, and 100% speed.

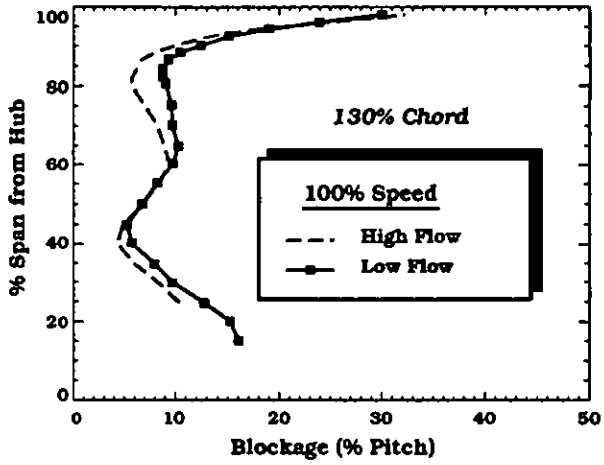

Figure 8 Radial distribution of Blockage at 130% chord and 100% speed for the low flow and high flow conditions.

Similarly, for the design speed data consider the following:

1. Blockage is significantly larger in the endwall region as compared to the core region.
2. Blockage in the endwall region is much larger at design speed than part speed conditions. The increase in blockage from part speed to design speed conditions is attributed to the increase in rotor tip clearance flow and the additional blockage resulting from the stronger interaction between the shock and the clearance flow.
3. The radial distribution of blockage in the core region is no longer constant with radius and the level is much larger than it was at part speed. Clearly, the blockage due to the rotor wakes at design speed is significantly larger in comparison to that of the wakes at part speed conditions.

Comparisons of Design Speed Results at High and Low Flow. The impact of varying the loading while maintaining a nearly constant inlet relative Mach number on blockage development is illustrated in Figure 8, where the radial distributions of blockage for the high and low flow conditions are plotted. The measurements at the high flow condition were acquired with the same resolution in the radial direction as that indicated by the symbols at the low flow condition. As the loading is increased from the high flow to low flow condition the overall blockage increases as expected. However, the increase in blockage is not uniform across the span. From Figure 8 it is evident that the blockage increase primarily occurs from 60–90% span and below 40% span. It is also interesting to note that the shape of the curve representing the radial distribution of blockage is similar for the high and low flow conditions at design speed and very much different from that at part speed conditions.

Summary of Blockage Results Downstream of the Blade Row. Table 2 summarizes the blockage calculations downstream of the blade row. The last two columns of this table were generated by performing an integration of the radial distribution of the blockage in the core flow and endwall regions. For example the average blockage in the endwall region is evaluated by:

$$B|_{r_1-r_2} = \frac{\int_{r_1}^{r_2} \delta^*(r)\, dr}{\pi(r_2^2 - r_1^2)/NB} \qquad (7)$$

where r_1 and r_2 indicate the radii over which the blockage is evaluated and in this case are representative of the endwall defect region. From Table 2 it is evident that the integrated average of the blockage in the endwall defect region increases as the increase in pressure difference across the blade tips increases with rotational speed. Also, the blockage in the core flow region at design speed is approximately double that at part speed conditions. In the next section the flow physics responsible for these trends in blockage development will be discussed.

Table 2 Summary of Integrated Blockage Results Downstream of the Rotor

% Design-Speed	Flow Rate	Endwall Defect Region (% span)	Endwall Blockage (% area)	Core Flow Blockage (% area)
100	High	84 - 98	17	8
100	Low	84 - 98	18	10
80	High	86 - 98	14	4
60	High	86 - 98	10	4

Relating Blockage to Rotor Flow Physics

In this section we will verify that the radial distributions of blockage depicted in Figures 7 and 8 are related to the flow physics of the rotor. Specifically, the sensitivity of blockage to the shock strength and its interaction with the blade surface boundary layer and the rotor tip clearance flows will be demonstrated using experimental data. First, the relationship between the radial distribution of blockage to the pressure and temperature distribution will be discussed.

Impact of Blockage on Performance. The radial distribution of total pressure ratio and total temperature ratio for the rotor operating conditions corresponding to the circled data points in Figure 2 are presented in Figure 9. The data are plotted on different scales but with the same sensitivity so comparisons could be made between operating conditions. The shape of the radial distribution of total temperature ratio and total pressure ratio is similar at 60% and 80% speed and very much different from that at design speed, which is consistent with the distributions of blockage plotted in Figure 7. In the core flow region, an increase in blockage results in an acceleration of the flow and a reduction of the work input. Therefore, an increase in blockage results in a reduction of core-flow temperature rise to the fluid and conversely, a decrease in blockage results in an increase of core-flow temperature rise. For example, at design speed the blockage dips to a local minimum at 40% span which is compatible with a local increase in the total pressure and total temperature i.e. less blockage implies more work input and therefore more pressure rise. Similarly, at part speed conditions the pressure ratio and temperature ratio from 20% to 80% span varies linearly across the passage and the distributions of adiabatic efficiency (not shown) are nearly equal, which is consistent with the linear and nearly uniform distributions of blockage in the core flow region. In addition, the reduced levels of adiabatic efficiency at design speed (as compared to part speed conditions — see Figure 2) is in agreement with the increase in blockage across the span at design speed relative to that at part speed conditions. Therefore, the blockage, as calculated herein, is not only consistent with the overall performance characteristics, but it also is consistent with the radial distributions of pressure and temperature.

Endwall Region : Impact of Shock / Vortex Interaction. In this section it will be shown that the increase in blockage in the endwall, as depicted in Figures 7 and 8, is directly related to the blockage associated with the tip clearance flow and the additional blockage resulting from the interaction of the tip leakage flow with the passage shock. A detailed discussion of the endwall flow physics for this rotor is presented in Suder & Celestina (1996), and therefore only a brief discussion of their results which pertain to blockage development is included herein.

A description of the blade-to-blade flow field along the 95% span streamsurface is depicted by contours of the relative Mach number for the rotor operating at design speed high flow and low flow conditions in Figure 10. Note that the tip clearance height within which the clearance vortex originates is approximately 0.5% of span. Therefore, the Mach contours in Figure 10 at 95% span indicate the influence of the tip clearance flow which lies below the actual tip clearance region. As the rotor back pressure is increased (from high flow to low flow condition) the Mach contours at midpitch and 20% of rotor chord become more distorted due to a strengthening of the interaction between the clearance vortex and the passage shock. Downstream of the shock/vortex interaction, a region of low relative Mach number exists due to the blockage generated by the diffusion inherent to the vortex passing through the steep pressure gradient associated with the shock. The data indicate that the low Mach number fluid within the diffused vortex migrates toward the pressure surface and merges with the rotor wake. Using the location of the lowest Mach number to indicate the 'heart' of the blockage region and the level to represent the severity, it is evident that the blockage

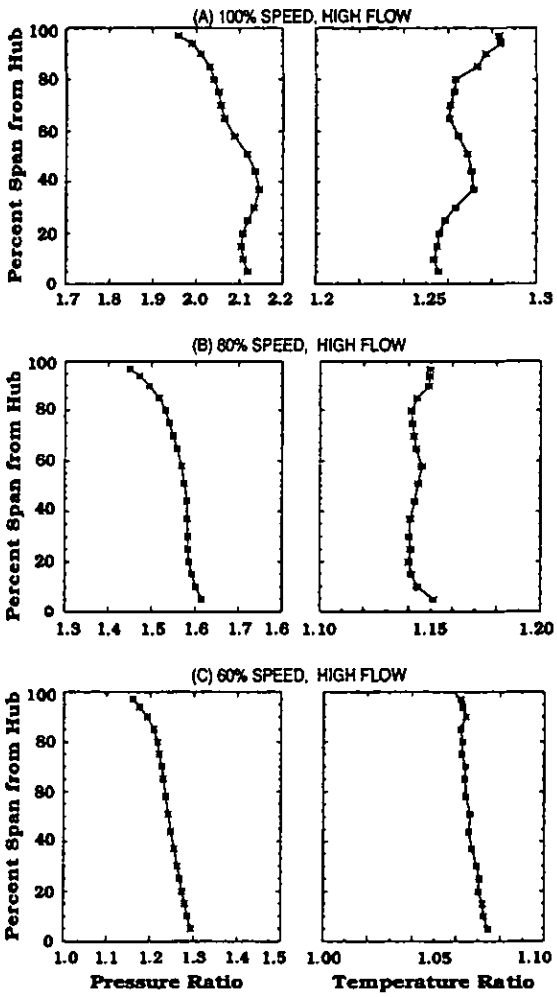

Figure 9 Radial distributions of the overall performance characteristics at a) 100% speed, b) 80% speed, and c) 60% speed for the rotor operating along a throttle line.

becomes more severe and is located further upstream as the rotor backpressure is increased from the high flow to the low flow operating conditions.

A comparison of the endwall flowfield at 80% speed to that at design speed indicates a similar path of the vortex trajectory. Likewise, the interaction between the clearance vortex and the shock occurs near 20% chord and midpitch, and downstream of the shock vortex interaction resides a region of low Mach number fluid which migrates towards the pressure surface and merges with the rotor wake. In summary, at 80% speed the blockage generated by the shock / vortex interaction is consistent with the design speed results at a reduced shock strength. Similarly, at 60% speed, in the absence of the shock, the blockage in the endwall region decreases with decreased loading. These results are in agreement with Khalid's (1994) correlation of endwall blockage versus loading.

Comparison with Khalid's Correlation. Khalid (1994) evaluated the blockage in the endwall region from CFD solutions of a low speed stator, low speed rotor, and a transonic fan using several values of tip clearance heights. He developed non-dimensional parameters

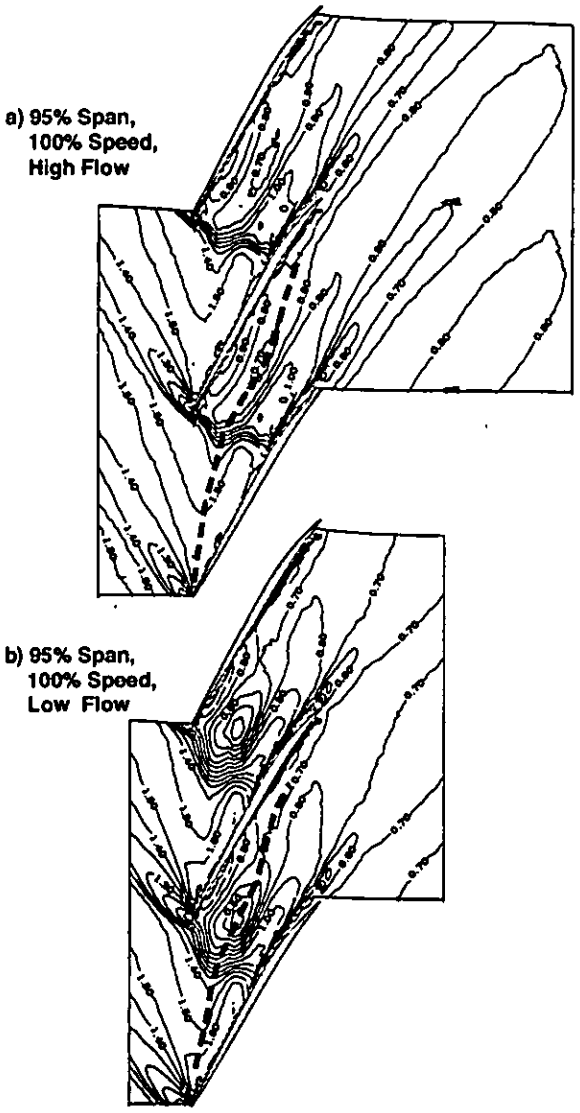

Figure 10 Contours of the relative Mach number in a blade-to-blade view along the 95% streamsurface for design speed (where · — — — indicetes trajectory of tip leakage vortex).

representing the endwall blockage and aerodynamic blade loading and showed that the results from all of his computations were well correlated. The blockage parameter can be summarized as:

$$\frac{blocked\ area\ in\ the\ endwall}{leakage\ flow\ area} * \frac{\Delta P\ in\ through\ flow\ direction}{\Delta P\ across\ blade\ tip} \tag{8}$$

where the second term is the ratio of the pressure difference which drives the mainflow through the passage to the pressure difference which drives the leakage flow through the clearance height. The loading parameter is the ratio of the relative dynamic head integrated over the defect region in the endwall to the inlet relative dynamic head evaluated at the radial reference location corresponding to two times the clearance height from the endwall. Khalid's results illustrate the increase in the endwall blockage with increased loading and indicate that there is a limiting value of the loading parameter.

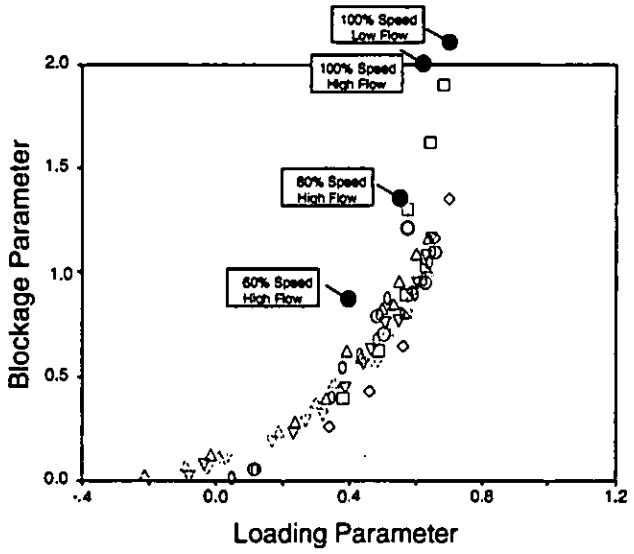

Figure 11 Comparison of NASA rotor 37 data to Khalid's correlation of loading versus endwall blockage.

For this investigation the data acquired downstream of the blade row were normalized in a manner analogous to Khalid's blockage and loading parameters and the results are presented in Figure 11 where the values for NASA rotor 37 are denoted by the flagged solid circles and all other symbols represent results from Khalid's computations. The general trend of the correlation is preserved in that the data exhibits the increase in endwall blockage with loading and is in agreement with Khalid's limiting value for the loading parameter. In conclusion, the increase in the endwall blockage, as determined from the experimental measurements and indicated in Figures 7 and 8, is consistent with an increase in blade loading.

Core Flow Region: Influence of Shock / Boundary Layer Interaction. The blade to blade flow field at 70% span for the rotor operating at design speed and low flow condition is presented in terms of measured relative Mach number contours in Figure 12. Figure 12b features a blowup of the leading edge region of Figure 12a. The shock forms in the front of the blade and is detached. Downstream of the shock in front of the leading edge the flow is subsonic and there is a rapid acceleration around the leading edge of the blade on the suction surface. The flow continues to accelerate on the suction surface until it encounters the shock from the adjacent blade. The shock strength is reasonable for a nearly normal shock as indicated by an upstream Mach number of 1.4–1.45 and a downstream Mach number of 0.7–0.8. (At an upstream Mach number of 1.4 a normal shock results in a post-shock Mach number of 0.74.) Also shown in Figure 12b is the interaction region between the rotor passage shock and the suction surface boundary layer. Since the boundary layer fluid cannot sustain the steep pressure gradient resulting from a nearly normal shock, the flow field adjusts and the shock becomes more oblique near the blade surface, thereby forming a lambda (λ) shock. Downstream of the lambda shock is evidence of a thickening of the blade suction surface boundary layer. Downstream of the shock and especially near the trailing edge it is evident that the suction surface boundary layer is considerably thicker than the pressure surface boundary layer.

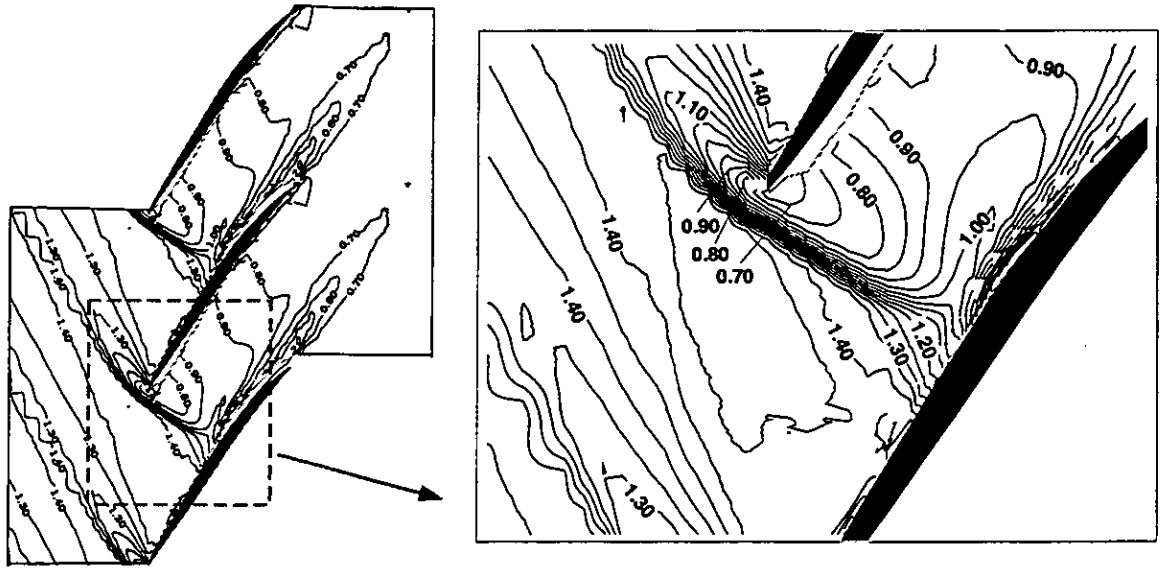

a) 70% Streamsurface b) Shock / Boundary Layer Interaction Region

Figure 12 Contours of measured relative Mach number along the 70% span streamsurface for the rotor operating at design speed and low flow condition.

The impact on blockage due to reducing the strength of the passage shock is best illustrated by comparing the rotor wakes at 100% and 80% speed at the high flow condition, as shown in Figure 13. The inlet relative Mach number at 70% span has decreased from 1.4 at design speed to 1.1 at 80% speed. It is evident that decreasing the shock strength from 100% speed to 80% speed at the high flow condition results in a significant change in the boundary layer development and the blockage associated with the rotor wake.

Likewise, a comparison of the rotor wakes at 80% and 60% speed (not shown here) indicates the width and depth of the rotor wakes are nearly identical in character and much reduced in comparison to design speed. This indicates that the shock / boundary layer interaction was sufficient to thicken the suction surface boundary layer at design speed but not by a measurable amount below 80% speed. Therefore, the difference in the blockage between the design speed and part speed conditions in the core flow region, shown in Figure 7, is due to the additional blockage generated by the stronger shock / boundary layer interaction on the blade suction surface at design speed.

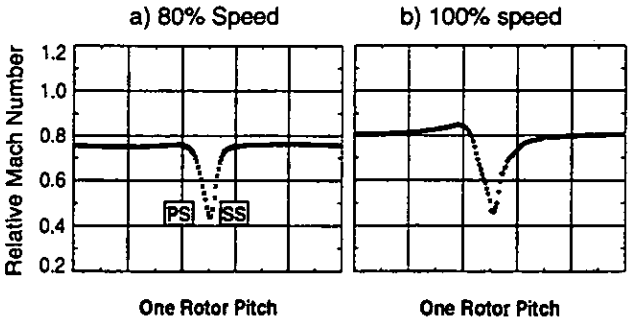

Figure 13 Relative Mach number distributions on the 70% span streamsurface for the rotor operating near peak efficiency.

Blockage Development within the Rotor Passage

It has been shown that the increased blockage in the core flow region at design speed is associated with the additional blockage resulting from the shock / boundary layer interaction. The question is how much of the blockage is due to the shock boundary layer interaction itself and how much results from diffusing a thicker boundary layer downstream of the shock boundary layer interaction region. In order to answer these questions, we will investigate the blockage development within the rotor passage.

The blockage on the blade suction surface was calculated on the 70% span streamsurface for the rotor operating at design speed low flow condition, and these results are presented in Figure 14. The region of the shock boundary layer interaction is identified by the region denoted 'lambda shock region'. In this region there is strong evidence to suggest the presence of a lambda shock (see Figure 12), and it was quite difficult to define the edge of the boundary layer. It is evident that the increase in blockage that occurs across the shock, for which blockage increases by a factor of 10, is much more significant than the blockage increase due to diffusion downstream of the shock, for which blockage increases by a factor of 1.5–2. Therefore, the shock/boundary layer interaction dominates the generation of blockage in the core flow region. This same development of blockage was evident at other spans as well. A relevant question is whether the shock / boundary layer interaction is sufficient to separate the blade surface boundary layer.

Results from wind tunnel tests on flat plate turbulent boundary layers will be used to determine if the suction surface boundary layer is separated. Using separation criteria deduced from flat plate results is justified because the geometry and the flow over the first part of the blade suction surface of the airfoil section at 70% span resembles that of a flat plate geometry and flow structure. The suction surface angles indicate very little turning over the front part of the

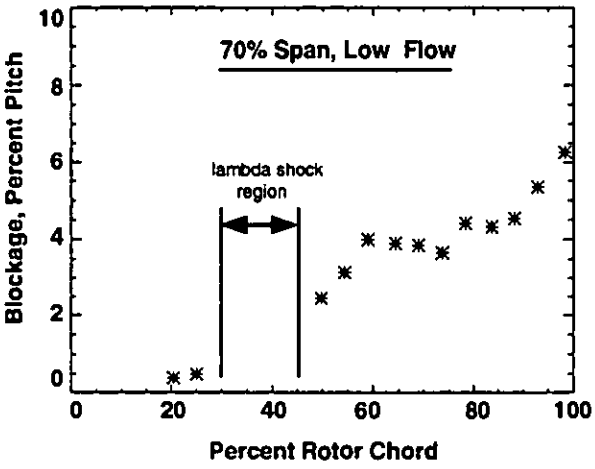

Figure 14 Blockage development on the blade suction surface at 70% span for low flow condition at design speed.

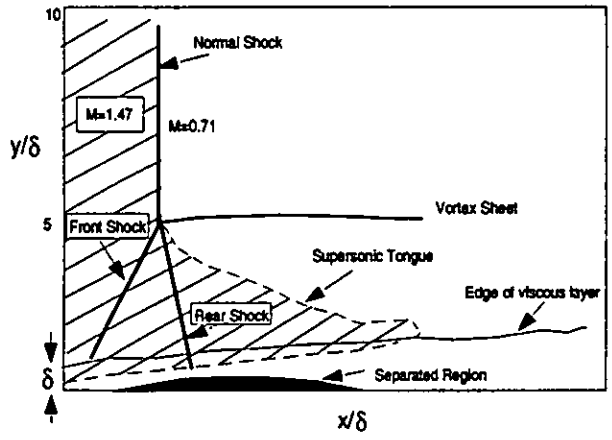

Figure 15 Seddon's model depicting the boundary layer separation due to a normal two-dimensional shock wave.

airfoil prior to the shock impingement on the suction surface. In addition, the distribution of the relative Mach number near the blade surface indicates a nearly zero velocity gradient prior to the shock impingement on the suction surface.

Seddon's model (Seddon, 1960) depicting the boundary layer separation due to a normal two-dimensional shock wave is presented in Figure 15. The normal shock is bifurcated into a classical lambda (λ) shape close to the surface. The front leg of the lambda shock is formed in response to the separation bubble and directs the flow away from the surface. The rear leg of the lambda shock deflects the flow back into the mainflow direction. A vortex sheet is shed downstream of the bifurcation point due to the entropy differences of the flow region behind the normal shock and the two oblique shocks. For the rotor geometry in question the Reynolds number based on chord is about $1.8X10^6$ and the boundary layer thickness ahead of the shock is approximately 4% of pitch. Therefore, it is anticipated that the separated region, if it exists, is much too small to measure. However, according to Seddon's model the lambda shock structure extends to a distance from the wall which is 5 times the boundary layer thickness and measurements were acquired in this region. In order to assess if the severity of the shock / boundary layer interaction is sufficient to cause a separation, the data was examined for evidence of the flow angle changes inherent to a lambda shock where the front oblique shock turns the flow away from the surface and the second or rear oblique shock re-directs the flow in the mainflow direction. Alber et al. (1973) has shown that the boundary layer is separated if the flow undergoes a deflection angle greater than 6.6 degrees.

The flow deviation from the blade surface angle is plotted for the high flow and low flow conditions at design speed in Figure 16. The flow in general follows the pressure surface, whereas on the suction surface there are regions where the flow deviates from the blade surface angle. Near mid-chord there are regions of increasing and decreasing deviation which suggest flow turning through the front and rear legs of a lambda shock. At the low flow condition there is an increase in the suction surface deviation angle from 35% to 45% chord followed by a decrease in the deviation from 45% to 50% chord. This region from 35% to 50% chord corresponds to the region of the shock influence on the blade suction surface as depicted in the blade surface Mach number distributions in Figure 12 and the blockage distribution in Figure 14. Similarly, at the high flow there is an increase in the deviation from 45% to 55% chord and a subsequent decrease in deviation from 55% to 65% chord, which also corresponds to the region of the shock influence on the blade suction surface. These changes in the flow deflection are near the value of 6.6 degrees required for boundary layer separation. Unfortunately the data near the blade surface is not sufficient in detail to detect the size of the separation. Similar results (not shown) were found for the 30% and 50% span streamsurfaces at design speed high and low flow operating conditions.

Results at Part Speed Conditions. Attempts to calculate the blockage development inside the blade for the data at part speed conditions were unsuccessful because the thickness of the boundary layer downstream of the shock was much reduced at part speed and the data was not of sufficient quality to evaluate the boundary layer displacement and momentum thicknesses. However, there was sufficient data to deduce the edge of the boundary layer, and therefore the deviation from the blade surface angles was evaluated. The results for 85% speed and 80% speed conditions are presented in Figure 17. Except for the last 20% of blade chord on the suction surface it is evident that the flow follows the blade surfaces. At 85% speed there is evidence of an increase and decrease in deviation from 45% to 55% chord which corresponds to the location of the shock impingement and influence on the blade suction surface. However the flow deflection is less than three degrees and according to Alber et al. (1973) is not sufficient to indicate a separation. In contrast, at 80% speed there is no evidence of the increase and decrease in deviation due to a lambda shock. Therefore, based on the distribution of the deviation from the blade surface angles, it is concluded that the shock is not of sufficient strength to separate the blade suction surface boundary layer at 80% and 85% speed.

Variation of Blockage with Span at Design Speed. It is reasonable to ask why the radial distribution of blockage varies so unpredictably across the span at design speed. One would suspect that if the additional blockage, relative to that at part speed conditions, results from the shock induced boundary layer separation then the blockage

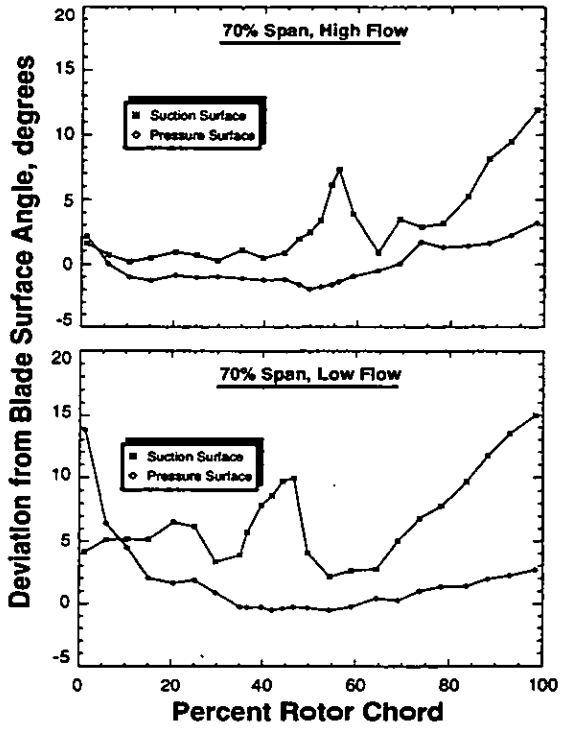

Figure 16 Deviation from blade surface angles on the 70% span streamsurface at high flow and low flow conditions at design speed.

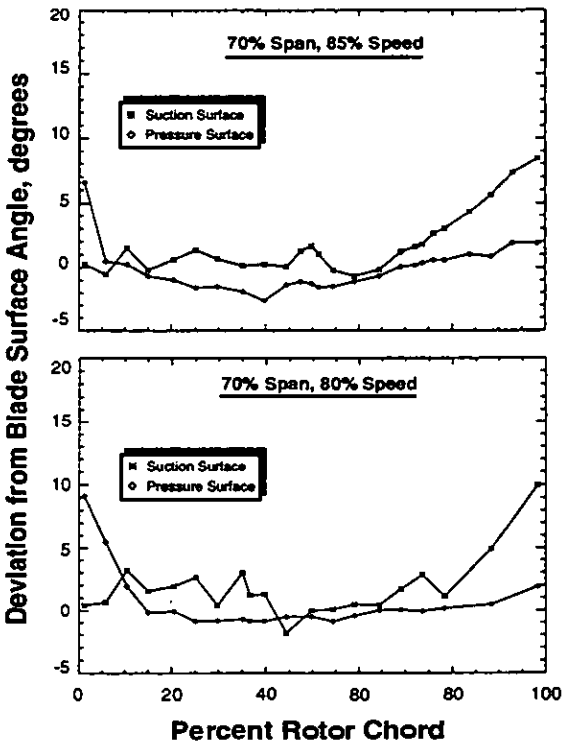

Figure 17 Deviation from blade surface angles on the 70% span streamsurface at 85% speed and 80% speed.

would increase with increasing inlet relative Mach number, and therefore, the blockage would merely increase with span. However, the blade camber decreases with span such that at the lower spans the camber results in a flow acceleration along the suction surface of the blade. The pre-shock Mach number at lower spans is therefore comparable to that at the higher blade spans. To determine the spanwise variation in shock strength, the Mach number normal to the flow was estimated from measured Mach numbers and flow angles upstream and downstream of the shock as prescribed in detail by Suder (1996). The results indicated that the normal Mach number ranged from 1.3–1.4 for the design speed cases at all measured spans and was less than 1.3 (max of 1.27 at 85% speed) for all part speed cases. From wind tunnel tests (Nussdorfer, 1956, Atkin and Squire, 1992, Alber et al., 1993, and Chriss, 1987) it has been shown that the pressure rise associated with a normal shock Mach number of around 1.3 is required to separate the boundary layer. Therefore deducing from the level of the estimated normal Mach number and the plots of deviation from the blade suction surface, the shock strength is sufficient to separate the boundary layer over much if not all of the blade span at design speed.

The blockage generated by the shock / boundary layer interaction is a function of the shock strength, location of where the shock impinges on the blade suction surface, the boundary layer thickness prior to the shock, and the pressure gradient downstream of the shock / boundary layer interaction region (see Griepentrog, 1972, Ackeret et al., 1947, Liepmann, 1946 , and Pearcy, 1959). When the shock separates the boundary layer, the blockage is quite sensitive to these effects, and it is much less sensitive when the boundary layer is not separated as is evident in Figure 7. Unfortunately, the data is not sufficient to accurately describe 1) the boundary layer characteristics upstream of the shock impingement on the suction surface where the boundary layer is very thin, 2) the details of the flow within the shock / boundary layer interaction region and therefore the size of the separation, and 3) the radial migration that results within the low momentum and/or separated regions. However, the data does indicate the boundary layer is separated at 30%, 50%, and 70% span at design speed, and therefore, the variation in blockage in the core flow region at design speed may be attributed to the spanwise variation of shock strength, size and location of the separation, blade suction surface curvature, and the pressure gradient to which the boundary layer is subjected.

To illustrate that the spanwise variation of blockage is directly related to the details of the blade boundary layer characteristics and shock / boundary layer interaction process, in the absence of detailed data in the shock / boundary layer interaction region, the blockage was evaluated using the results from two CFD simulations. The two simulations employed an identical algorithm and computational grid, and the only difference between the simulations was the turbulence model used. One computation used a modified Baldwin-Lomax turbulence model (Celestina, 1997) and Adamczyk et al., 1989) and the second computation used a modified two equation turbulence model as described by Shabbir et al. (1996). The radial distribution of blockage was evaluated using the same calculation procedure as described in the data analysis section, and a comparison of the CFD results with the data is presented in Figure 18. From this figure it is evident that the blockage levels calculated using the two-equation turbulence model are very much different from those using the Baldwin-Lomax turbulence model, and the two equation

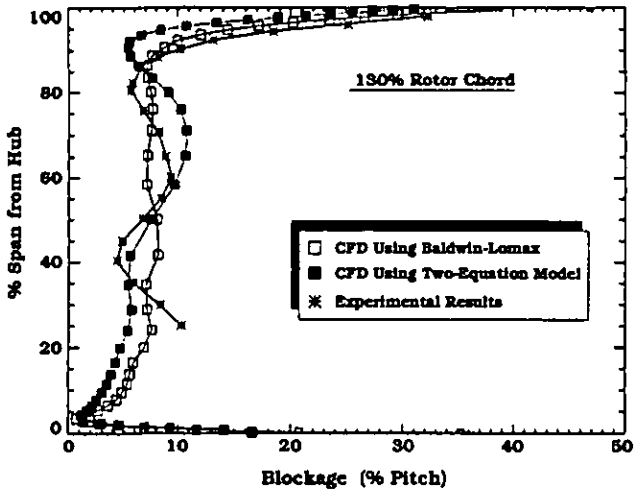

Figure 18 Radial blockage distribution at 130% chord for design speed and high flow condition — comparison between data and two CFD simulations.

model identifies a local increase in blockage from 40% to 80% span in agreement with the data. Further interrogation of the CFD simulations indicated that this local increase in blockage from the two equation model is primarily due to additional low momentum fluid on the blade suction surface which results from the shock / boundary layer interaction. In summary, the point of this discussion is not to compare the two turbulence models, but rather to demonstrate that 1) the spanwise variation in the blockage at 130% chord is primarily attributed to the spanwise variation in the blockage resulting from the shock / boundary layer interaction process within the blade passage, and 2) predicting the boundary layer characteristics and fluid mechanic details of the shock / boundary layer interaction is paramount to accurately predict the blockage and therefore the performance of this rotor.

CONCLUDING REMARKS

A detailed experimental investigation to understand and quantify the development of blockage in the flow field of a transonic axial flow compressor rotor has been undertaken. Comparisons of the blockage development at 60%, 80% and 100% speed at a constant incidence angle provided a means to evaluate the effect of variations of the inlet Mach number on the blockage development. Data acquired at design speed at varying rotor exit pressures provided a means to evaluate the sensitivity of blockage to changes in shock structure at a nearly constant inlet Mach number.

The conclusions of this investigation regarding the development of blockage in a transonic axial compressor are:

1. The radial distribution of the blockage was consistent with the radial distribution of the pressure and temperature rise across the rotor. For example, in the core-flow region a local increase in blockage coincided with a local decrease in the temperature and pressure rise and conversely, a region of reduced blockage coincided with a region of increased pressure and temperature rise.
2. Blockage in the endwall region was 2–3 times greater than that in the core flow region. The increase in blockage near the endwall is primarily attributed to the tip clearance flow and the shock / tip leakage vortex interaction. In addition, the blockage in the endwall region increases with blade loading in agreement with Khalid's (1994) correlation of endwall blockage versus aerodynamic blade loading.
3. In the core flow region at design speed conditions the blockage is more than double that at part speed conditions for the same incidence. This increase in blockage at design speed occurs because the shock / boundary layer interaction induces separation of the blade suction surface boundary layer.

It is clear that the performance of the rotor used in this investigation is very sensitive to changes in blockage and that the blockage related losses account for a significant amount of the total loss. It is believed that this sensitivity results from the high loading levels, high Mach numbers and tight choke area margin (A/A^* of 1.03 to 1.05) associated with this rotor. The sensitivity of the rotor performance to changes in blockage at design speed accompanied with the fact that the shock is of sufficient strength to separate the boundary layer provides a challenge to computational fluid dynamics codes used for design and analysis. As the design trends move to higher blade loadings and rotational speeds the shock strengths and flow phenomena reported herein will be more prevalent. Therefore, in order to optimize the design of compressors with high loading levels and tip speeds comparable to or in excess of the compressor rotor used in this investigation, it is paramount to be able to predict and/or model the blockage in order to accurately predict the rotor flowfield and performance.

ACKNOWLEDGMENTS

The author wishes to acknowledge the efforts of Dr. Tony Strazisar, Mr. Jerry Wood, and Dr. John Adamczyk of NASA Lewis Research Center for their guidance not only in the writing of this paper, but also for the many helpful discussions throughout the course of this work. I am also grateful to Dr. Ed Greitzer of Massachusetts Institute of Technology, Dr. Nick Cumpsty of Whittle Labs at Cambridge University, Dr. Frank Marble, Professor Emeritus from California Technology Institute, and Dr. Eli Reshotko from Case Western Reserve University for their helpful comments and suggestions. The author also would like to thank Mr. Mark Celestina of NYMA Inc. and Dr. Aamir Shabbir of Institute for Computational Mechanics in Propulsion for providing their computational results of NASA Rotor 37.

BIBLIOGRAPHY

Ackeret, J., Feldmann, F.,, and Rott, N., 1947, "Investigation of Compression Shocks and Boundary Layers in Gases Moving at High Speed," *NACA TM 1113*.

Adamczyk, J., Celestina, M., Beach, T.,, and Barnett, M., 1989, "Simulation of Three-Dimensional Viscous Flow Within a Multi-Stage Turbine," *ASME Journal of Turbomachinery*, Vol. 112, no. 3, pp. 370–376.

Alber, I., Bacon, J., Masson, B.,, and D.J., C., 1973, "An Experimental Investigation of Turbulent Transonic Viscious-Inviscid Interactions," *AIAA Journal*, Vol. 11, no. 5, pp. 620–627.

Atkin, C., and Squire, L., 1992, "A Study of the Interaction of a Normal Shock Wave with a Turbulent Boundary Layer at Mach Numbers between 1.3 and 1.5," *European Journal Meachanics B/Fluids*, Vol. 11, no. 1.

Celestina, M. Personal communication —Provided computational results for NASA Rotor 37., 1997.

Chima, R., 1996, "Calculation of Tip Clearance Effects in a Transonic Compressor Rotor," ASME 96-GT-114 and accepted for publication in the Journal of Turbomachinery. Also NASA TM 107216.

Chriss, R., Keith, T., Hingst, W., Strazisar, A.,, and Porro, A., 1987, "An LDA Investigation of Three-Dimensional Normal Shock-Boundary Layer Interactions in a Corner," *AIAA-87-1369*.

Dalbert, P., and Wiss, D., 1995, "Numerical Transonic Flow Field Predictions for NASA Compressor Rotor 37," *ASME 95-GT-326*.

Denton, J., September, 1996, "Lessons learned from Rotor 37," *Presented at the Third International Symposium on Experimental and Computational Aerothermodynamics of Internal Flows (ISAIF)*.

Griepentrog, H., 1972, "Shock Wave Boundary Layer Interaction in Cascades," *Agardograph No. 164 an Boundary Layer Effects in Turbomachines*, edited by J. Surugue, North Atlantic Treaty Organization (NATO), Advisory Group for Research & Development (AGARD), pp. 443–456.

Khalid, S., 1994, *The Effects of Tip Clearance on Axial Compressor Pressure Rise*, Ph.D. Dissertation, Massachusetts Institute of Technology.

Koch, C., 1981, "Stalling Pressure Rise Capability of Axial Flow Compressor Stages," *ASME Journal of Engineering for Power*, Vol. 103, pp. 645–656.

Koch, C., and Smith, L., 1976, "Loss Sources and Magnitudes in Axial-Flow Compressors," *ASME Journal of Engineering for Power*, Vol. 98, pp. 411–424.

Liepmann, H., 1946, "The Interaction between Boundary Layer and Shock Waves in Transonic Flow," *Journal af Aeron. Sciences*, Vol. 13, no. 12.

Moore, R., and Reid, L., 1980, "Performance of Single-Stage Axial-Flow Transonic Compressor with Rotor and Stator Aspect Ratios of 1.19 and 1.26, Respectively, and with Design Pressure Ratio of 2.05," *NASA TP 1659*.

Nussdorfer, T., 1956, "Some Observations of Shock-induced Turbulent Separation on Supersonic Diffusers," *NACA RM E51 L26*.

Pearcey, H., 1959, "Some Effects of Shock Induced Separation of Turbulent Boundary Layers in Transonic Flow Past Aerofoils," *A.R.C. R&M*, no. 3108.

Reid, L., and Moore, R., 1978, "Design and Overall Performance of Four Highly Loaded, High-Speed Inlet Stages for an Advanced High-Pressure Ratio Core Compressor," *NASA TP 1337*.

Schlichting, H., *Boundary-Layer Theory*, Seventhth ed., McGraw-Hill, 1979.

Seddon, J., March, 1960, "Flow Produced by Interaction of a Turbulent Boundary Layer with a Normal Shock Wave of Strength Sufficient to Cause Separation," *Brit. Aero. Res. Council Report and Memo No. 3502*.

Shabbir, A., Zhu, J.,, and Celestina, M., 1996, "Assessment of Three Turbulence Models in a Compressor Rotor," *ASME paper 96-GT-198*.

Smith, J. L.H., 1970, "Casing Boundary Layers in Multistage Axial-Flow Compressors," *Flow Research on Blading*, edited by A. L. S. Dzung, Elsevier. , pp. 275–304.

Strazisar, A., Wood, J., Hathaway, M.,, and Suder, K., 1989, "Laser Anemometer Measurements in a Transonic Axial-Flow Fan Rotor," *NASA TP 2879*.

Suder, K., and Celestina, M., 1996, "Experimental and Computational Investigation of the Tip Clearance Flow in a Transonic Axial Compressor Rotor," *Journal of Turbomachinery*, Vol. 118, no. 2, pp. 218–229.

Suder, K. L., 1996, *Experimental Investigation of the Flow Field in a Transonic, Axial Flow Compressor with Respect to the Development of Blockage and Loss*, Ph.D. Dissertation, Case Western reserve University. also NASA TM 107310.

Urasek, D., and Janetzke, D., 1972, "Performance of Tandem-Bladed Transonic Compressor Rotor with Rotor Tip Speed of 1375 Feet per Second," *NASA TM X-2484*.

Wood, J., Strazisar, A.,, and Simonyi, P., 1986, "Shock Structure Measured in a Transonic Fan using Laser Anemometry," *AGARD CP-401: Transonic and Supersonic Phenomena in Turbomachines*, AGARD (Advisory Group for Aerospace Research and Development) of the North Atlantic Treaty Organization.